The Local Field Potential Reflects Surplus Spike Synchrony

Michael Denker[1], Sébastien Roux[2], Henrik Lindén[3], Markus Diesmann[1,4], Alexa Riehle[2] and Sonja Grün[1,4,5]

[1]RIKEN Brain Science Institute, Wako-shi, Saitama 351-0198, Japan, [2]Mediterranean Institute of Cognitive Neuroscience (INCM), Centre National de la Recherche Scientifique—University Aix-Marseille 2, 13402 Marseille Cedex 20, France, [3]Department of Mathematical Sciences and Technology, Norwegian University of Life Sciences, 1432 Ås, Norway, [4]Institute of Neuroscience and Medicine (INM-6), Research Center Jülich, 52425 Jülich, Germany and [5]Bernstein Center for Computational Neuroscience, 10115 Berlin, Germany

Address correspondence to Dr. Michael Denker, RIKEN Brain Science Institute, 2-1 Hirosawa, Wako-shi, Saitama 351-0198, Japan. Email: mdenker@brain.riken.jp.

While oscillations of the local field potential (LFP) are commonly attributed to the synchronization of neuronal firing rate on the same time scale, their relationship to coincident spiking in the millisecond range is unknown. Here, we present experimental evidence to reconcile the notions of synchrony at the level of spiking and at the mesoscopic scale. We demonstrate that only in time intervals of significant spike synchrony that cannot be explained on the basis of firing rates, coincident spikes are better phase locked to the LFP than predicted by the locking of the individual spikes. This effect is enhanced in periods of large LFP amplitudes. A quantitative model explains the LFP dynamics by the orchestrated spiking activity in neuronal groups that contribute the observed surplus synchrony. From the correlation analysis, we infer that neurons participate in different constellations but contribute only a fraction of their spikes to temporally precise spike configurations. This finding provides direct evidence for the hypothesized relation that precise spike synchrony constitutes a major temporally and spatially organized component of the LFP.

Keywords: motor cortex, oscillation, population signals, synchrony

Introduction

Ongoing efforts to unravel the mechanisms governing brain processing have led to the proposal that information is conveyed by the coordinated firing patterns of specific subgroups of neurons. Efforts to prove or disprove this hypothesis concentrate on detecting precise synchrony (Riehle et al. 1997; Shlens et al. 2006; Ohiorhenuan et al. 2010) or more complex spatiotemporal patterns (Ikegaya et al. 2004, Shmiel et al. 2005) exhibited by the spiking activity of the network ensemble. On the other hand, oscillations observed in electrophysiological recordings on a mesoscopic scale, such as the local field potential (LFP), hint at synchronization within the population activity on a slower time scale. In this paper, we establish the experimental finding that such oscillatory network activity is related in a nontrivial fashion to action potentials that exhibit synchronization on a fast time scale and discuss a potential mechanism and functional interpretation.

It is commonly accepted that the LFP reflects synaptic activity impinging on neurons in the vicinity of the recording electrode. This assumption is rooted in the biophysical explanation of the LFP as a spatially weighted average of the synaptic transmembrane currents (Mitzdorf 1985; Viswanathan and Freeman 2007). Indeed, recent studies have demonstrated that the LFP at a given location may be well predicted by the spiking activity of neurons recorded in a large area surrounding the field potential electrode by using their postsynaptic signatures obtained as spike-triggered LFP averages as a kernel (Nauhaus et al. 2009). This view is supported by the finding that the LFP is highly correlated with the membrane potential fluctuations of nearby neurons (Poulet and Petersen 2008) even in the absence of spiking activity in the recorded cells (Okun et al. 2010). In consequence of this evidence, the oscillatory structure observed ubiquitously in the LFP is hypothesized to reflect predominantly synchronized inputs (Elul 1971; Logothetis and Wandell 2004). Nevertheless, although the natural extension from synchronization on the level of the membrane potential to that of spiking activity is on everybody's mind, the correspondence is not straightforward (Poulet and Petersen 2008).

Synchronization in the synaptic drive is likely to influence the probability of spike generation with respect to the LFP. Indeed, a large body of literature investigates the relationship of single spikes and the LFP. To date, it has been established that neural spiking activity may become transiently entrained to the LFP in a regular or irregular fashion (Eckhorn and Obermueller 1993; Murthy and Fetz 1996b). The degree of phase locking between neurons and the LFP typically increases with the strength of beta/gamma LFP oscillations (Denker et al. 2007). Such oscillatory periods are correlated with stimulus features (Engel et al. 1990) as well as top-down processes, such as attention (Fries et al. 2001), and are thus believed to be computationally relevant (e.g., Harris et al. 2002; Friedrich et al. 2004; Fries et al. 2007; Montemurro et al. 2008; Tiesinga and Sejnowski 2009).

The high degree of correlation of membrane potentials recorded from close-by neurons (Lampl et al. 1999) and the similarity of LFPs taken at distant recording sites (Destexhe et al. 1999) suggests that these oscillatory network fluctuations revealed in the LFP act as average input in a neuron-unspecific manner. Indeed, neurons tend to comodulate their firing probabilities: cross-correlations between simultaneously recorded neurons tend to show a periodic structure during oscillatory episodes of the LFP (Murthy and Fetz 1996b). Moreover, if the level of rate correlation in neuronal ensembles is high then the firing rate profiles correlate well with gamma band LFP power (Nir et al. 2007), while exhibiting a characteristic phase relationship with the LFP (Womelsdorf et al. 2007). Therefore, during oscillatory LFP periods it is expected that neurons exhibit covarying firing rates on the time scale of the LFP cycle and that the resulting spike coincidences should exhibit a phase relationship to the LFP explained by the degree of phase locking of the individual neurons. Much less clear is the expectation on the behavior of synchronized action potentials that are not explained by the firing rates (e.g., Riehle

et al. 1997; Kilavik et al. 2009) in relation to the LFP oscillation. Poulet and Petersen (2008) succeeded to directly demonstrate that synchronized slow subthreshold membrane potential oscillations that correlate with the LFP do not imply the output action potentials to be synchronized. This discrepancy between subthreshold dynamics and spiking activity is in agreement with theoretical work linking subthreshold and suprathreshold dynamics (Tetzlaff et al. 2008). The findings of Poulet and Petersen (2008) rather indicate that the occurrence of action potentials is governed by strong, precisely timed, neuron-specific inputs to the cells, suggesting these as additional independent activity riding on the oscillation. A recent study by Okun et al. (2010) adds support to this view by suggesting that their data can be understood if precise firing occurs due to input from smaller groups of neurons as opposed to slower network-wide population activity. Thus, such specific inputs may exhibit only a subtle representation in the LFP.

One hypothesis compatible with such input characteristics states that the network dynamics involves the activation of a specific set of common inputs triggering a precise synchronous discharge within a defined group of neurons, termed the Hebbian cell assembly (Hebb 1949). On the spiking level, the hallmark signature of an activated assembly is the functionally coordinated synchronous spiking with millisecond precision observed in parallel recordings of neuronal activity (Gerstein et al. 1989) that exceeds the expectation based on the firing rates (Aertsen et al. 1989). It is shown that not only LFP oscillations correlate with external stimuli (e.g., Engel et al. 1990), behavioral aspects (e.g., Scherberger et al. 2005), and internal processes (e.g., Murthy and Fetz 1996a; Donoghue et al. 1998; Roux et al. 2006; Saleh et al. 2010) but also surplus precise spike synchrony is observed and modulated in a functional context (Vaadia et al. 1995; Riehle et al. 1997; Kilavik et al. 2009). Early on, it has been conjectured that LFP oscillations may represent an alternative, network-averaged signature of such assembly activations (Eckhorn et al. 1988; Gray et al. 1989; Donoghue et al. 1998; Singer 1999). In support of this perspective, it was shown that the occurrence of distinct spatially organized spiking activity across neurons combined with their phase relationship to LFP oscillations encode a substantial amount of surplus of information about the stimulus compared with information contained in the firing rate alone (Kayser et al. 2009). Nevertheless, it remains an open question if LFPs reflect more than synchronization due to an underlying rate modulation, and if these oscillations may provide a framework for the occurrence of precisely coordinated spiking as predicted by an active assembly (Buzsáki 2004; Jensen 2006; Canolty et al. 2010).

In this study, we uncover the missing critical link between surplus spike synchrony considered as assembly expressions and LFP oscillations by directly relating these 2 observables on a trial-by-trial basis. For this purpose, we concentrate on recordings from motor cortex of behaving monkey, for which spike synchrony (Riehle et al. 1997) as well as LFP oscillations (Murthy and Fetz 1992; Kilavik et al. 2010) have been shown to be behaviorally relevant in tasks involving movement preparation. Therefore, we identify transient periods where the spiking activity of simultaneously recorded neurons shows a surplus of coincidence events compared with the number expected on the basis of the firing rates using the Unitary Events (UEs) analysis method (Grün et al. 2002a, 2002b; for a schematic illustration, see Fig. 1). During these periods, the excess

synchrony is attributed to the synchronous firing of observed neurons as part of a network process that reliably coactivates a specific subset of neurons with respect to a given time point: the assembly (Fig. 1; spikes colored green and blue). We show that synchronous spikes originating from transient assembly activation exhibit pronounced phase locking to the LFP that exceeds the locking of coincidences that occur by chance. The results enable us to embed the notions of LFP oscillations and transient spike synchrony into a single framework and estimate the fractional contribution of assemblies to neuronal activity, exploiting signatures of assembly activity on the spike and the LFP level. Revealing that assembly activity detected as a significant surplus of spike synchrony correlates not only with behavior but also with a mesoscopic brain signal corroborates its relevance in cortical processing. Our findings reinterpret the dynamical features of the LFP in terms of neuronal processing and open a new perspective for decoding of an accessible and reliable signal in brain–machine interfaces and diagnostics.

Materials and Methods

Ethics Statement
Care and treatment of the animals during all stages of the experiments conformed to the European and French government regulations, according to the Weatherall report ("The use of non-human primates in research," December 2006).

Experimental Design and Electrophysiological Recordings
All data were taken from recordings partially presented elsewhere (Roux et al. 2006; Kilavik et al. 2009). Two rhesus monkeys (monkey K and monkey O) were trained to perform arm movements from a center position to 1 of 2 possible peripheral targets left and right of the center in 2 different tasks involving an instructed delay. In the first, a choice reaction time task (chRT), both peripheral targets were presented simultaneously as a preparatory signal (PS), one in red and the other in green. The animal learned to attribute to each color 1 of 2 possible delay durations. If the (directionally noninformative) auditory response signal (RS) occurred after a short delay, the monkey had to select the red target, after a long delay the green one. Both, the laterality of the colored targets and the presentation of the 2 durations were varied at random with equal probability. In contrast, in the second, self-paced movement task (SELF), the presentation of only one peripheral target, either in red or in green, either at the left or at the right, required a self-initiated response after estimating 1 of the 2 delays as coded by PS. In both tasks (Roux et al. 2006), 4 different timing patterns were used to identify the temporal duration of the short and long delay, respectively: 1) 500 and 1000 ms (monkey K); 2) 500 and 1200 ms (monkey K); 3) 600 and 1200 ms (monkey O); and 4) 1000 and 1400 ms (monkey O).

In this study, we exclusively analyze the delay activity, that is, activity recorded during the preparatory period (PP) starting at PS and ending with either RS in the chRT task or in the earliest allowed response time (AT) in the SELF task. Therefore, the trials were aligned to PS occurrence for the analysis. The neural activity related to movement execution, that is, after RS or AT, respectively, is not analyzed. For both tasks, only correct trials are considered, in which the monkey responded within a time window (after the end of PP) of maximally 300 (monkey O) and 500 ms (monkey K) and in which movements were performed in the required movement direction.

In order to exclude effects due to pooling of neuronal activities of different behavioral contexts and different tasks, their activity is analyzed independently for the 4 possible behavioral conditions (combinations of short- or long-delay duration and left or right upcoming movement direction) and each experimental session. For the sake of simplicity, we refer in this manuscript to a recorded neuron by the combination of its identity and the behavioral context during which it was recorded. In this sense, data recorded from the same
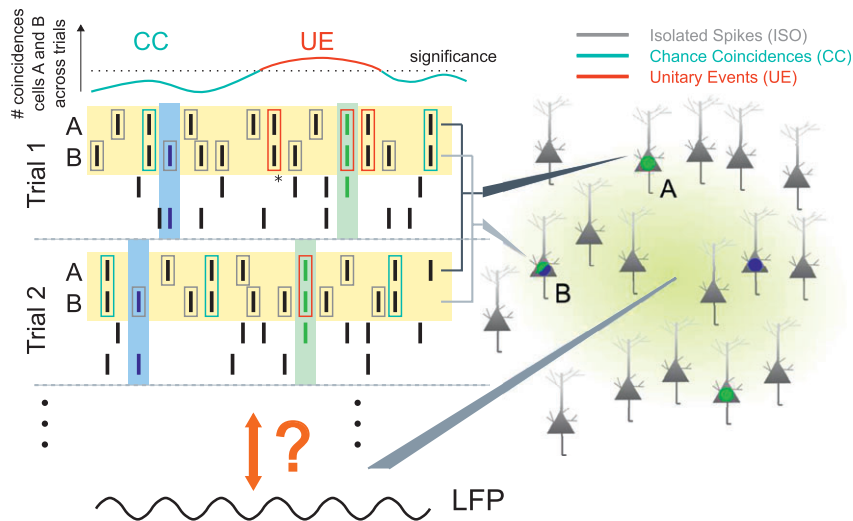
Figure 1. Schematic illustration of the analysis framework. Spikes of 2 neurons (A and B, yellow background) and an LFP are recorded in 2 trials from 3 separate electrodes (right) spaced at approximately 400 μm. In addition, spikes from 2 unobserved neurons are depicted. The spikes of one recorded neuron are classified as CC (cyan) or UE (red) if they are precisely (±3 ms) synchronized with a spike of the second neuron recorded in parallel, and otherwise as isolated (ISO, gray). In contrast to CCs, UEs identify coincidences in epochs where the high number of observed coincidences across trials (top left) significantly exceeds the prediction based on the firing rates. This study investigates the relationship of these 2 types of observed spike synchrony (CC and UE) to the LFP population signal as a mesoscopic monitor of brain processing. In UE epochs, synchrony between both neurons in excess of the chance contribution is commonly explained by their specific reliable and temporally confined coactivation in a neuronal ensemble, termed assembly. Two assembly activations are sketched in blue and green (colored spikes and background). Only one neuron (B) of the assembly shown in blue is observed; neuron A participates only in the assembly shown in green. Hence, only the assembly shown in green can be detected as a UE by the elevated coincidence count between A and B, yet also ISO and CC spikes may be part of an assembly hidden from the observer. Asterisk: see main text.

neuron may enter a population average up to 8 times (maximum of 4 different conditions in 2 tasks).

Data Acquisition and Data Analysis

LFPs and spikes were recorded simultaneously in primary motor cortex using a multielectrode device of 2–4 electrodes (MT-EPS, Alpha Omega). Spikes of single neurons were detected by an online sorting algorithm (MSD; Alpha Omega). The interelectrode distance is on the order of 400 μm. LFPs were sampled at a resolution of 250–500 Hz and hardware filtered (band pass, 1–100 Hz). In total, we analyzed 53 recording sessions (monkey K: 25; O: 28), which yielded 143 single neurons or 570 combinations of neurons and behavioral conditions. On average 33 ± 11 trials are recorded per experimental condition. We never combine LFP and spikes that are recorded on the same electrode to exclude the possibility of spike artifacts in the signal (Zanos et al. 2011). We consider this as justified since we confirmed that simultaneously recorded LFPs are highly synchronous in the frequency regimes of interest. Likewise, synchronous activity between neurons is analyzed only for neurons recorded from different electrodes, totaling 123 analyzed pairs of neurons. All data analysis is performed using the Matlab software environment (The Mathworks Inc.).

Coincidence Detection and UE Analysis

From simultaneously recorded spike data of individual sessions, we extract all unique pair combinations of spike trains that are recorded from distinct electrodes. In a first step, we compute the number of coincident spike occurrences of the pairs of neurons in a time-dependent manner (compare Supplementary Fig. S1). To allow coincidences with a temporal jitter up to a maximal coincidence width of $b = 3$ ms, we apply the "multiple-shift" approach (Grün et al. 1999; Grammont and Riehle 2003). In this method, exact coincidences (within the time resolution $h = 0.1$ ms of the data) are detected for a range of shifts between $-b$ and $+b$ of the second spike train against the first (reference) spike train. To account for the nonstationarity of the neurons' firing rates, and to capture the dynamics of correlation, we perform the UE analysis in a sliding window fashion (Grün et al. 2002b). This is done by moving a window of fixed duration (here: $T_w = 100$ ms)

along the data to cover the duration of a trial, that is, the duration of the PP. The length of the time window is therefore chosen large enough to include at least one complete cycle of LFP oscillations in the beta range. The window is advanced in steps corresponding to the time resolution h of the data. The first window position is centered at trial onset and the last window at the end of the delay period.

Within each window position, the total number of empirical coincidence counts n_{emp} is derived by summing the exact coincident spike events from each shift l and from all M trials j: $n_{emp} = \sum_{j=1}^{M} \sum_{l=1}^{L} n_{emp}^{j,l}$, with $L = 2(b/h) + 1$. To derive UEs, this count is compared with the number of coincidences that would occur by chance given the firing rates of the neurons. This involves the following calculations. To account for nonstationary rates across trials (Grün et al. 2003), the relevant measures are obtained from the single trial and only subsequently summed across trials. Thus, within the analysis window, the expected number of coincidences is calculated on the basis of the trial-by-trial firing probabilities $p_{i,j}$ which are estimated by the spike count $c_{i,j}$ of neuron i in trial j divided by the number of bins N within a window: $p_{i,j} = c_{i,j}/N$ with $N = T_w/b$. The joint probability for finding a coincidence by chance per trial is calculated by the product of the single-neuron firing probabilities $p_{12,j} = p_{1,j}p_{2,j}$. The expected number of coincidences per trial j results from multiplying this probability by the number of bins N that are included in the analysis window and the number of shifts L: $n_{exp}^{j} = NLp_{12,j}$. The total number of expected coincidences within the window is derived from the sum of the expected numbers per trial: $n_{exp} = \sum_{j=1}^{M} n_{exp}^{j}$.

Finally, we compare the empirical n_{emp} to the expected number n_{exp} of coincidences to detect significant deviations. To this end, we calculate the joint p value jp, that is, the probability of measuring the given number of empirical coincidences (or an even larger number) under the null hypothesis of independent firing. The distribution under this null hypothesis representing the probability to find a given number of coincidences is given analytically assuming Poisson processes (Grün et al. 1999). The latter assumption is shown to yield a conservative estimate for cortical spike trains considering their non-Poisson and nonrenewal properties (Grün 2009). Then the significance of n_{emp} yields (Grün et al. 2002a): $jp(n_{emp}|n_{exp}) = \sum_{n_{exp}}^{n_{emp}} \frac{n_{exp}^{r}}{r!} e^{-n_{exp}}$. If its value is below an a priori threshold (here chosen as 5%) coincident firing is classified as significant and identified as UEs. Spikes are detected as UE if they are

part of a coincidence and in at least one sliding window identified to contain significant excess synchrony (for an illustrated summary of this analysis approach, see Maldonado et al. 2008). In addition, we require such time windows to exhibit a minimum firing rate of 5 Hz for each neuron. If several neurons are recorded in parallel, a spike is labeled as UE if it is part of a UE coincidence in at least one of the analyzed pairs. Spikes that are part of coincident events but not identified as UE with respect to any of the neurons recorded in parallel are labeled as chance coincidences (CC), all remaining spikes as isolated spikes (ISO). By this definition, the spikes of each neuron receive exactly one label and enter all subsequent analyses once. For the analysis presented in Supplementary Fig. S2, a UE section is defined as all time bins belonging to a consecutive sequence of analysis windows (length T_w) that are classified as significant; a CC section is constructed by grouping all remaining time bins into contiguous segments.

Cross-Correlation Analysis

To calculate the cross-correlogram in Figure 2, we first construct vectors x_n^j and y_n^j of the spike trains by binning (1 ms bin width, index n, length N) of each trial j of the 2 neurons. The cross-correlogram is constructed across the M trials for a time lag $\tau \geq 0$ (in bins) as $C_{xy}(\tau) = \sum_{j=1}^{M} \sum_{n=0}^{N-\tau-1} x_{n+\tau}^j y_n^j$ and for $\tau < 0$ as $C_{xy}(\tau) = C_{yx}(-\tau)$. To compensate for a bias due to the decrease of available data as τ increases, we correct each bin of $C_{xy}(\tau)$ by a factor of $1/(N-|\tau|)$, which is particularly important for small N. The raw correlogram is then normalized to 1 at lag $\tau = 0$ by multiplying by a factor of $N/\sqrt{n_1 n_2}$, where n_1 and n_2 are the spike counts across trials of neurons 1 and 2, respectively. To evaluate the significance of observed cross-correlations, we compute bin by bin the mean and variability (2 standard deviations) resulting from 1000 cross-correlograms obtained by an identical analysis of surrogate spike trains. Each surrogate is constructed by randomly displacing (dithering) each spike of the original spike train homogeneously by maximally ±10 ms (Hatsopoulos et al. 2003). This procedure maintains the structure of correlation due to slow rate nonstationarity while destroying potential excess precise synchronization of spikes. The autocorrelograms (Fig. 2 and Supplementary Fig. S2) of a spike train x_n^j are calculated in the same fashion using $y_n^j = x_n^j$.

Spectral Analysis

Power spectra are used to assess the dominant frequencies in the LFP. All power spectra are calculated using a Hamming window as taper. To illustrate the temporal modulation of power in different frequency bands, we use a time-resolved spectral analysis using 200 ms windows with a 50 ms overlap.

Spike-Triggered Averages

Spike-triggered averages (STAs) are computed by averaging LFP segments from time windows of 200 ms centered at each spike time. For the STA analysis, LFPs are filtered with a lower cutoff frequency of 2 Hz to remove DC components and an upper cutoff frequency of 80 Hz. To compare STAs across recordings, in which electrode signals may differ in their absolute amplitude values, we z-transform each LFP before further analysis by subtracting its mean and dividing by its standard deviation (each calculated across trials). In order to quantify the magnitude (or size) of an STA, we calculate the total area the STA encloses with the time axis. Similar results to those presented here (not shown) are obtained using alternative measures of the STA magnitude, such as the area under its envelope (cf. phase analysis), or the maximum of its absolute value. The variability of the STA is in general dependent on the number of trigger spikes. In order to compare STAs obtained from 2 sets of trigger spikes of different numbers of spikes n_1 and n_2 ($n_1 > n_2$), we construct 1000 STAs of set 1, each computed from n_2 randomly selected spikes. We define the STA of set 2 to be larger than that of set 1 if the magnitude of set 2 exceeds $\rho = 50\%$ of the recomputations of set 1 and significantly larger (at a level of 5%) if it exceeds $\rho = 95\%$ of the recomputations. Thus, this comparison is based exclusively on the magnitudes of the 2 STAs and therefore does not consider any model-based dependencies between the sets of STAs.

Rate-Amplitude Correlation

To assess the degree of correlation between LFP oscillation strength and spike rate (Fig. 3D), we calculate the mean value of the rectified z-transformed LFP of each trial in sliding windows of 200 ms length and 100 ms overlap. These values are then correlated with the rate profile of the neuron estimated as the spike count pooled across trials in the same sliding windows. Similar results as those shown here are obtained using alternative measures of LFP strength, including the mean value of the envelope of the beta-filtered signal (cf. phase analysis) or by using the total signal power in the beta range (10–22 Hz).

Peak-Triggered Spike Histograms

We evaluate the population-averaged spiking discharge triggered on the peaks of the LFP oscillation (Fig. 3E; cf. also Destexhe et al. 1999). To this end, we detect maxima of the LFP separated by a minimum time interval of 33 ms, which corresponds to a maximal oscillation frequency of 30 Hz and allows singling out the oscillatory component in the beta frequency range. In detail, all maxima are detected and ordered by signal amplitude. Starting from the highest amplitude, maxima are selected for the analysis as long as they are separated by at least 33 ms from any previously chosen maximum with higher amplitude. The histogram is calculated from spike data within a window of 200 ms around each trigger peak and averaged across all individual peaks in all neurons (for a different technique to relate spike times to electroencephalography time course based on amplitude, see Eeckman and Freeman 1990). Simultaneously, we also compute the peak-triggered LFP by averaging the z-transformed LFP aligned on its peaks.

Phase Analysis

Based on the dominant beta frequencies obtained on a session-by-session basis, z-transformed LFPs of both monkeys are filtered with a zero-phase 10–22 Hz band-pass filter (Butterworth, 8-pole). Short filter transients in the time domain allow for good estimates of the instantaneous LFP amplitude. In a subsequent step, we calculate the instantaneous phase of the LFP from the analytic signal $\xi(t) = x(t) + i\tilde{x}(t)$ obtained via the Hilbert transformation $\tilde{x}(t) = \frac{1}{\pi} \text{P.V.} \int \frac{x(t)}{t-\tau} d\tau$ of the original signal $x(t)$, where P.V. denotes that the integral is to be taken as Cauchy principal value (Le Van Quyen et al. 2001). In this formalism, troughs of the LFP are identified by a phase of π. The calculation of the analytic signal can be applied to arbitrary signals, but its interpretation as instantaneous phase is difficult where either the signal amplitude becomes too small to discriminate the oscillation from background noise or where the regular oscillation is disrupted (Boashash 1992). To account for these effects, we discard phase values which violate the monotonicity of the phase time series or exhibit instantaneous phase jumps. To further corroborate our results, we exclude from our analysis those 10% of spikes per neuron that occur at the lowest LFP amplitudes.

We analyze the distributions of extracted phase values at the times of spike occurrences (Denker et al. 2007) using tools from circular statistics (Mardia and Jupp 2000). The mean phase ϕ is obtained via the circular average $Re^{i\phi} = N^{-1} \sum e^{i\phi(t_i)}$, where $\phi(t_i)$ indicates the phase of the field potential at time t_i of spike i. Furthermore, we utilize the transformation of the vector strength R to the circular standard deviation $\sigma = \sqrt{-2 \log R}$ as a measure of the concentration of the phase distribution. For small values, σ relates to the standard deviation of a normal distribution, whereas for flat distributions $\sigma \to \infty$. In all phase analyses, we discard neurons that fire in total (across trials) less than 25 spikes.

Additionally, we employ 2 measures to quantify whether spikes recorded from individual neurons show a significant phase preference to the LFP. For the first, we test against the null hypothesis that the phase sample is taken from the uniform circular distribution (Rayleigh test, cf. Mardia and Jupp 2000), which is expected by assuming a regular (e.g., filtered) field potential and independent random spiking. However, spike trains that have a certain regular structure in time may display intrinsic locking to the LFP. To measure the degree of genuine locking that is not explained by the regularities of the 2 signals, we calculate as the second measure the degree of locking R in 1000 surrogates, each created by shuffling the interspike intervals of the
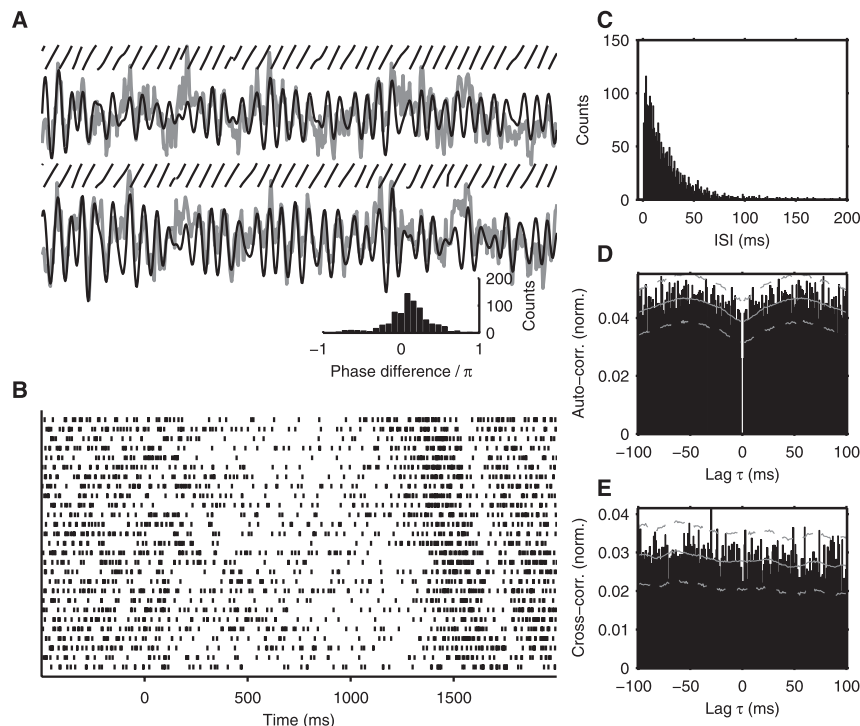
Figure 2. Characteristics of LFP and spiking dynamics. (*A*) Two single-trial LFPs recorded simultaneously (gray) at different electrodes (during long trials with movement to the right in the SELF task). Superimposed are the beta-filtered (10–22 Hz) signals (black) and their instantaneous oscillation phase (indicated by small black lines above). The histogram visualizes the phase differences between the 2 signals across all time bins. (*B*) Spike raster of all trials (sorted by reaction time after the delay period) of one example neuron recorded in the same session as the LFPs shown above. (*C–E*) Corresponding interspike interval distribution (*C*), the normalized autocorrelogram (*D*), and the cross-correlogram (*E*) with a different neuron recorded in parallel (neuron 1 in Supplementary Fig. S1). Gray curves in *D* and *E* indicate the mean (solid) and 5% confidence intervals (dashed) of the autocorrelogram and cross-correlogram obtained from 1000 surrogate spike trains where each spike was dithered uniformly in a window of ±10 ms around its original position. The structure of the autocorrelation and cross-correlation is explained by the nonstationarity of the firing rate. The center bin is removed in (*D*). bin size in all panels: 1 ms.

spikes on a trial-by-trial basis (random placement of the first spike). This procedure preserves to first order the regularity manifested in the interspike interval distribution. A comparison with the measured value *R* yields the *P*-value for this surrogate test. Since the construction of such surrogates can only be performed on the complete spike train, this measure could not be sensibly applied to the subsets of spikes in our analysis (i.e., ISO, CC, UE, as well as Lo and Hi used in the amplitude analysis).

The phase distributions of spike coincidences (e.g., CC and UE distributions of Figs 5 and 6) may be trivially sharpened due to a preferred phase occurrence of individual spikes. To correct for this effect, we calculated the expected phase distribution of coincident spikes (black curve in Figs 5 and 6 as well as Supplementary Fig. S5). To this end, we calculate the joint phase probability distribution of a neuron pair by the phase-by-phase multiplication of the occurrence probabilities of spikes at these phases. The predictor (labeled Ψ_{PHASE}) for the whole population is the average of these pairwise phase distributions each weighted by the relative number of coincidences between the corresponding 2 neurons.

In contrast to this predictor which considers the phase of spikes irrespective of the spike interval distribution, we also construct a second predictor (labeled Ψ_{ISI}) based on the reverse scenario. For each pair of simultaneously recorded neurons, the interspike intervals of the spike trains of each neuron are shuffled on a trial-by-trial basis to create a set of 1000 surrogate pairs. For each surrogate, the variance σ is evaluated separately for the resulting sets of noncoincident and coincident spikes. Thus, we obtain for each neuron the variances σ of phase locking of coincident and noncoincident spikes for the original data and for the 1000 surrogates, allowing us to compare their distributions (Fig. 4*C*).

Results

Synchrony-Based Spike Classification

We analyze spike data of 143 single units and simultaneously recorded LFP data from motor cortical areas in 2 monkeys during the instructed delay (PP) of 2 motor tasks (see Materials and Methods). Both spike synchrony (Kilavik et al. 2009) and LFP oscillations in the beta band (Murthy and Fetz 1996a; Kilavik et al. 2010) have been shown to be behaviorally relevant to movement preparation. LFPs and spikes were recorded from electrodes spaced at 400 μm (for a schematic illustration, see Fig. 1) to exclude trivial signal correlations induced by volume conduction effects (cf., e.g., Katzner et al. 2009). In these recordings, there is in general no intuitive correspondence between spatially synchronized (Fig. 2*A*; cf. also Rubino et al. 2006) LFP oscillations and precise spike synchronization in the absence of a network oscillation in the spiking activity: the autocorrelation and cross-correlation structures of single units (Fig. 2*B–E*) tend to exhibit a flat structure in the sense that all their features are fully explained by predictors that preserve the rate fluctuations (cf. also Murthy and Fetz 1996b; for an analysis of spike train variability in comparable data, see Nawrot et al. 2008).

In a first step, we characterize the synchronization between all neuronal pairs on a fine temporal scale. To this end, we
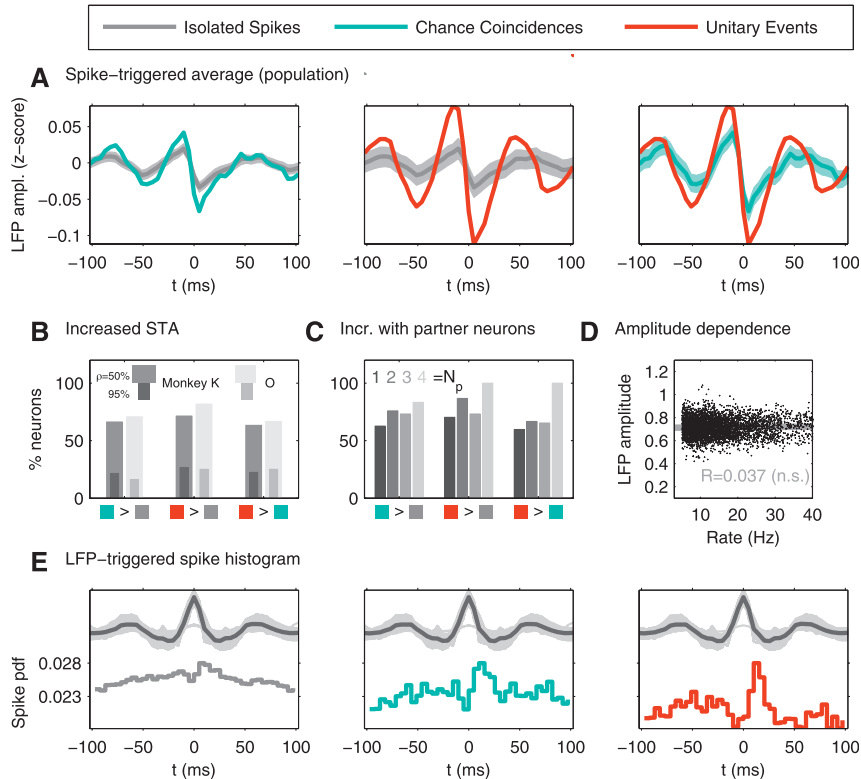
Figure 3. The magnitude of the STA depends on the occurrence of synchronized spiking activity. (*A*) STA of the LFP averaged over all 123 neurons (*n* = 297 484 spikes total) for the 3 disjunct sets of spikes. The left panel compares STAs of ISO (dark gray curve, *n* = 240 455) with CC (cyan curve, *n* = 44 867). To account for the difference in variability due to sample sizes, the STA of ISO is repeatedly recomputed using only 44 867 random trigger spikes. The light gray band encloses at each point in time 95% of all recomputed STAs. The middle and right panel compare STAs of UE (red curve, *n* = 12 162) with ISO and CC, respectively. (*B*) Percentage of neurons per animal (vertical) where the STA obtained from one spike set exceeds (in area) the STA of another set (horizontal axis: the 3 comparisons of sets corresponding to the 3 graphs in *A* are represented by the color codes). Wide, light bars: For each neuron the STA of one set qualifies as larger than the other if it exceeds ρ = 50% of its 1000 sample size corrected recomputations (performed as in *A*). Superimposed narrow dark bars: more strict criterion ρ = 95% (i.e., at α = 5%). (*C*) Same comparisons as in *B*, however, now the 4 bars of each comparison distinguish STAs obtained for neurons with the same number N_p of partner neurons tested for pairwise coincidences (ρ = 50%; pooled across both animals). (*D*) The correlation of LFP amplitude and spike rate (200 ms windows, 100 ms overlap) is not significant (α = 0.05, coefficient *R*). (*E*) Bottom: LFP-triggered histogram of ISO (left), CC (middle), and UE (right) averaged across the population (expressed as the probability of spike occurrence). The trigger times are all local LFP maxima, which are separated by a minimum time difference of 33 ms (i.e., allowing trigger frequencies of up to 30 Hz to single out the beta component). Each neuron is related to exactly one LFP signal. Top: LFP averages based on the same triggers shown for each neuron (light gray curves). The dark gray curve is the average of the single-neuron LFP averages.

identify time windows where the spiking activity of simultaneously recorded sets of neurons shows a surplus of coincidence events across trials compared with the number expected on the basis of the firing rates using the UE analysis (Grün et al. 2002a, 2002b). During these periods, we attribute the excess synchrony of both observed neurons to a network process that reliably activates a specific subset of neurons: the assembly (Fig. 1 depicts the spikes of 2 different assemblies shown in green and blue, respectively). Based on this detection of precise spike synchrony (Grün et al. 1999) in all pairs of simultaneously recorded neurons, we classify a neuron's spikes (all spikes) exclusively into 1 of 3 sets: isolated spikes (ISO), chance coincidences (CC), and Unitary Events (UE). Spikes involved in pairwise coincidences (within 3 ms) are classified as CC if they occur during time periods (100 ms windows) where the observed coincidence rate is explained by the instantaneous trial-by-trial rates of the 2 involved neurons, and as UE if their number significantly exceeds the expectation (see Materials and Methods). When more than 2 neurons are recorded in parallel, a spike is labeled UE if it forms a (pairwise) UE coincidence with at least one of the simultaneously recorded neurons. Likewise, spikes that form CC coincidences but are not identified as UE in any neuron pair are labeled CC.

Finally, spikes not classified as CC or UE with respect to any of the simultaneously recorded neurons are classified as ISO. Consequently each spike is labeled according to the type of event it belongs to, and an individual spike train may contain spikes of different categories (compare gray, cyan, and red boxes around spikes in Fig. 1). In a given UE period, a distinction between coincidences stemming from the activation of the assumed assembly and those due to chance is not possible. Therefore, a substantial fraction (for an estimate, see Discussion) of coincidences in the UE group may still be due to chance coincident spiking (e.g., the leftmost UE coincidence of trial 1 marked by an asterisk in Fig. 1).

The classification of data sections into CC and UE periods is based solely on the occurrence of excess spike synchrony between neuronal pairs, yet other features of the recorded spike trains might also differ depending on this selection process. To test for this possibility, we performed a series of analyses separately for the CC and UE time periods. The duration of UE sections (for a definition, see Materials and Methods) composed of consecutive UE windows (136.0 ± 48.8 ms, all errors given as standard deviation; *n* = 840) is in general shorter than the duration of CC sections (485.1 ± 371.1 ms; *n* = 428), indicating their transient nature. In terms of firing
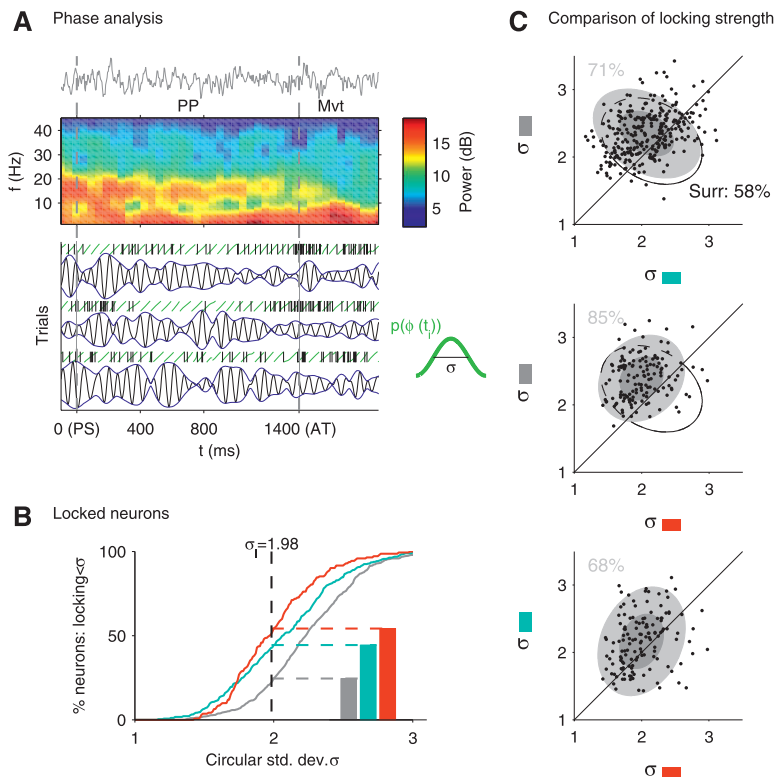
Figure 4. LFP-spike phase coupling reveals locking increase for coincidences. (*A*) Determination of phase and amplitude (example neuron). Top: single recorded LFP trial; middle: trial-averaged power spectrogram. The beta activity during the PP (between PS and AT) disappears with movement (Mvt). Bottom: For analysis, phase (green) and amplitude (blue) of the beta-filtered LFP (upper trial is shown in the top graph) is extracted at the spike times (ticks). Resulting phase distributions (green) are characterized by their circular standard deviation σ. Same neuron as in Figure 2. (*B*) Percentage of neurons with a circular standard deviation of the ISO (gray curve), CC (cyan), and UE (red) phase distribution below σ (horizontal axis). For the average $\sigma_l = 1.98$ of the set of significantly locked neurons (all spikes, $\alpha = 0.05$), the percentages are also shown as bars. (*C*) Comparisons of the circular standard deviations σ of the 3 sets for individual neurons: ISO versus CC (top, $n = 291$), ISO versus UE (middle, $n = 142$), and CC versus UE (bottom, $n = 136$). Each dot represents one neuron in one experimental configuration. The percentages show the fraction of data points above the diagonal. The light (dark) gray filled ellipse covers 2 (1) standard deviation(s) of the sample variance (outlined ellipse: predictor Ψ_{ISI}, surrogate data ISO vs. CC with shuffled ISIs).

rates (Supplementary Fig. S2*A1*), we observe no difference between CC (average: 17.5 ± 11.0 Hz) and UE windows (18.2 ± 10.1 Hz) throughout the population. Similarly, the pooled interspike interval distributions (Supplementary Fig. S2*A2*) obtained from individual analysis windows are comparable for CC and UE. Consistent with the UE analysis results, the average probability of 0.332 to observe a UE coincidence in a single trial within one analysis window is higher than the probability of 0.210 obtained for a CC coincidence (cf. Supplementary Fig. S2*A3*). These few coincidences are rather equally distributed across the trials (as opposed to occurring in rapid succession within a trial) in both CC and UE periods as indicated by the high probability to observe exactly one coincidence in a given trial (Supplementary Fig. S2*A4*) opposed to 2 or more coincidences. This observation strengthens the interpretation that the UE method detects a consistent coactivation of neurons across trials rather than a repeated coactivation within a trial. To test for changes in the regularity of the spike train, we quantify the amount variability of the interspike intervals by the coefficient of variation (CV) in CC and UE sections (Supplementary Fig. S2*B1*). The calculation of the CV is sensitive to the length of the data segments used for its estimation and hence the values obtained from the typically short sections are biased to lower values (cf., e.g., Nawrot et al. 2008; to highlight this fact, we choose to denote the coefficient as CV_{short}). Thus, to allow the comparison of the CV_{short} distributions obtained from CC and UE sections, we only

consider pairs of CV_{short} values from CC and UE sections of identical length (by cutting the longer of the 2 sections). As a result, we observe no difference of the CV_{short} distributions from spikes within CC and UE sections, allowing us to conclude that there is no particular degree of spike regularity in UE sections. As a control, we also show the distribution of CV_{short} obtained for Poisson spike trains (rates corresponding to the trial-average rate of UE sections) of the same lengths as the sections entering the histograms (blue curve, identical in both graphs). The resulting distribution is in strong agreement with the ones derived from experimental data, exhibiting the bias toward CV_{short} smaller than 1 (expected for infinite data length) due to short windows. Finally, the structure of the spike autocorrelogram is fully explained by the nonstationarity of the firing rates as indicated by the autocorrelations of surrogate spike trains in which the fine structure of spiking was destroyed by spike dithering (Supplementary Fig. S2*B2*). Further characterization of the occurrence of UEs in this data set can be inferred from Kilavik et al. (2009). Taken together, besides the fact that data segments differ in respect to the occurrence of excess synchrony, we observe no difference in the statistical features of the spike trains therein.

The Magnitude of Spike-Triggered LFP Averages Increases with Synchrony

As a first approach to the relation of the various spike types (ISO, CC, and UE) to the LFP, Figure 3*A* compares the STAs of

the LFP for the 3 sets. Each STA is pooled across all neuron–LFP pairs. We observe that the magnitude of the STAs of both, CCs (left, cyan) and UEs (middle, red), exceed that of the isolated spikes (gray). In order to account for random fluctuations in the magnitude of STAs that arise due to the different finite sample sizes of the ISO, CC, and UE groups, we tested that CC and UE STAs are significantly larger than resampled versions of the ISO STA constructed from the same number of spikes. Moreover, the STA of UE is larger than that of CC (right). The oscillatory structure of the STAs exhibits a strong beta frequency component, and the STAs are typically centered on the downward slope of the oscillation cycle. Although single-neuron STAs also exhibit these differences, they are more difficult to detect (for a typical example, see Supplementary Fig. S3). The reason for this is 2-fold: First, individual pairs exhibit a substantially higher sampling variance, especially considering the typically low number of UE spikes. Second, single-neuron STAs are more strongly influenced by variability in the instantaneous LFP frequency, the spike–LFP phase locking, and the oscillation amplitude. Nevertheless, we quantify the STA increase between the 3 sets of spikes for individual neurons using the area enclosed by the STAs and the horizontal axis as a measure for its magnitude (see Materials and Methods). Taking into account differences in the sampling variance by a resampling procedure, we show (Fig. 3B,C) the fraction of neurons where the STA of one set exceeds in magnitude the median of the resamples (ρ = 50%) or exceeds 95% of the resamples (ρ = 95%) corresponding to a significantly larger STA on a neuron-by-neuron basis with regard to sampling variability of the sets. In particular for UE spikes, the STA exceeds that of CC significantly (ρ = 95%) in a fraction of 23.7% of the single neurons of both monkeys (Fig. 3B). In contrast, in only 6.2% of neurons the opposite is true and the CC STA significantly exceeds that of UE (not shown as bar graph). For the other 2 comparisons, we obtain the following fractions of neurons (ρ = 95%): CC > ISO: 18.8%, ISO > CC: 3.4% and UE > ISO: 25.8%, ISO > UE: 2.9%. Taken together, we observe an increase of the STAs from ISO to CC to UE. Moreover, we find consistently more pronounced STAs for experiments where we are able to evaluate a larger number of partner neurons N_p for potential coincidences (Fig. 3C), thus better sampling the correlation structure of the neuronal population.

Three mechanisms could potentially underlie the differences in the STAs: changes in the instantaneous frequency of the dominant oscillatory component, in the LFP amplitude or in the locking between LFP and spikes. Regarding the first of these mechanisms, the oscillation observed in each of the 3 STAs exhibits the same frequency. Moreover, the 2 distributions of the instantaneous oscillation frequency of the beta-filtered signal measured in the center of each detected CC and UE section, respectively, are identical (Supplementary Fig. S2C1), independent of the filter details. Therefore, frequency variability does not explain the differences in the 3 STAs. For the remaining 2 mechanisms (amplitude and locking), the picture is much less clear. The LFP amplitude does not covary with the spike rate (Fig. 3D). Therefore, increased amplitudes and the disproportionate increase of the CC count during periods of elevated rates is an improbable cause of the STA increase for CC. Moreover, the amplitude (i.e., envelope) distribution of the beta-filtered LFP exhibits no clear differences between CC and UE sections (Supplementary Fig. S2C2). On the other hand, spike histograms triggered on the peaks of the LFP oscillations

(Fig. 3E) reveal that spikes do not only tend to prefer the falling phase but also avoid the rising phase of the LFP. Combined, this evidence seems to suggest that the 3 sets of spikes differ primarily in the degree of phase coupling to the LFP rather than in the accompanying amplitude of the LFP. However, on the basis of STA techniques alone, the 2 contributions cannot be clearly disentangled. In particular, these difficulties in interpreting the STA prevent us from constructing a predictor for the STAs of the coincident spikes (CC and UE) based on ISO spikes.

Increased Spike Synchrony Improves Spike–LFP Phase Coupling

In the following, we aim to obtain a more detailed picture regarding which of the 2 features of LFPs and spike trains (amplitude and phase coupling) are relevant in explaining the differences between the 3 STAs. In order to clearly differentiate between these mechanisms, it is necessary to formally disentangle the dependence of spike timing on the amplitude of the LFP from its dependence on the phase, which are obscured in the STA. By identifying these contributions individually, it will further become possible to make statistical predictions on dependencies between isolated spikes and coincidences in general (ISO vs. CC) and between CCs and excess synchrony in particular (CC vs. UE). Figure 4A explains the procedure (for details, see Materials and Methods). For both monkeys, we consistently observe a prominent beta oscillation (in both monkeys around 15–17 Hz) of the LFP during the PP that stops with movement onset (Mvt). Therefore, we focus on the beta frequency band by prefiltering the LFP for further analysis. We ensure that the employed filter band of 10–22 Hz, centered symmetrically on the mean beta frequency, captures the observed beta oscillation by comparing the resulting frequency composition (Supplementary Fig. S2C1) to that obtained for a wider and asymmetrical filter (8–30 Hz). We then extract the instantaneous phase and amplitude (envelope) of the filtered LFP for each spike time. We are now prepared to study the 2 contributions of phase and amplitude in detail across the population.

Figure 4B shows that across the population of neurons CC are systematically better locked (decreased circular standard deviation σ of the phase distribution) than ISO and UE better than CC. As a suitable reference value to compare the fraction of locked neurons in the 3 sets, we extracted the average locking strength σ_l = 1.98 (marked as a dashed line) obtained for those neurons that are significantly locked if all spikes are considered (ISI surrogate test for locking, see Materials and Methods). In the following, we investigate how the systematic differences in locking strength between the 3 sets of spikes are affected by the overall spike–LFP relationship of a particular neuron. To this end, we classify a neuron as strongly locked if the set of all its spikes exhibits significant locking to the LFP (ISI surrogate test). Nonsignificantly locked neurons are categorized as weakly locked. This differentiation (Supplementary Fig. S4A) between strongly (39%) and weakly (61%) locked neurons does not introduce a bias by affecting the percentage of neurons that contribute CC (strong: 55.0%; weak: 50.0%) and UE (strong: 28.4%; weak: 23.4%). Both groups exhibit the same general relation between ISO, CC, and UE (Supplementary Fig. S4B) as shown in Figure 4B. As expected, the percentage of neurons better locked than the chosen reference value σ_l in

the ISO group differs considerably (53% vs. 6%, gray bars in Supplementary Fig. S4B) between strongly and weakly locked neurons. However, this difference between strongly and weakly locked neurons is less pronounced for CCs (63% vs. 32%) and further decreases for UEs (65% vs. 46%). The conservation of the locking of UE spikes in strongly and weakly locked neurons compared with the declines for ISO and CC hints at different dynamical origins of the coincident spikes in CC and UE.

Figure 4C confirms that individual neurons are consistent with the findings for population ratios (Fig. 4B). The scatter plots of the circular standard deviation reveal that in 71% of the recorded neurons CC spikes are better locked than ISO spikes and in 85% of the neurons UE spikes are better locked than ISO spikes. Finally, in 68% of all neurons, UE spikes are better locked to the LFP than CC spikes. In contrast to the experimental data, only 58% of surrogate spike trains that retain the original interspike interval statistics (predictor Ψ_{ISI}, see Materials and Methods) show an increase in phase locking for coincident spikes (outlined ellipse). Indeed, compared with the STA analysis, even for individual neurons it is possible to detect differences between ISO, CC, and UE separately for the distribution of LFP phase (Fig. 5A, same example neuron as in Figs 2 and 4) and LFP amplitude (Fig. 5B).

The consistency in the population allows us to focus subsequent analyses on the phase locking of strongly locked neurons. The rationale is to reduce the differences in locking between the 3 sets of spikes to obtain a conservative estimate of the differences in their locking strengths (cf. Supplementary Fig. S4B). The corresponding phase distributions in the top graphs of Figure 6A constructed from all spikes of neurons that meet this selection criterion show that the locking to the LFP is strongest for UEs and weakest for isolated spikes. An even stronger discrepancy between the 3 distributions is observed when not constraining the analysis to the set of strongly locked neurons (Supplementary Fig. S5A).

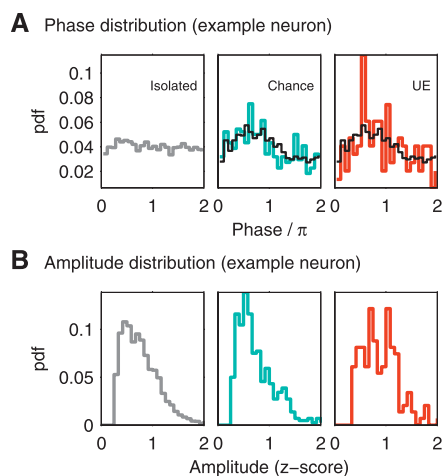The phase distribution exhibited by isolated spikes may equally be interpreted as a modulation of the spiking probability in time. Indeed, mapping LFP phase to time is supported by the high level of synchrony observed between LFPs from different electrodes (Fig. 2A). In consequence, the probability of observing a coincidence by chance is naturally determined by the individual phase-locking distributions of the 2 neurons forming the coincidence. One may therefore argue that the increased modulation of the phase distribution of CC is simply given as the joint phase distribution taken from both neurons (predictor Ψ_{PHASE} assuming independence of neurons, see Materials and Methods). Interestingly, the phase distribution of CC is indeed largely in agreement with this predictor (black curve in Fig. 5A and in the top graphs of Fig. 6A), while that of UE is not. By definition, UEs extract time windows with a high coincidence count and therefore could in principle be biased to detecting coincidences that occur in close temporal proximity. However, it is improbable that rapid sequences of UEs underlie the observed increase of locking strength since each UE window encompasses around 2 oscillation cycles of the LFP, and on average, we observe less than 1 coincidence
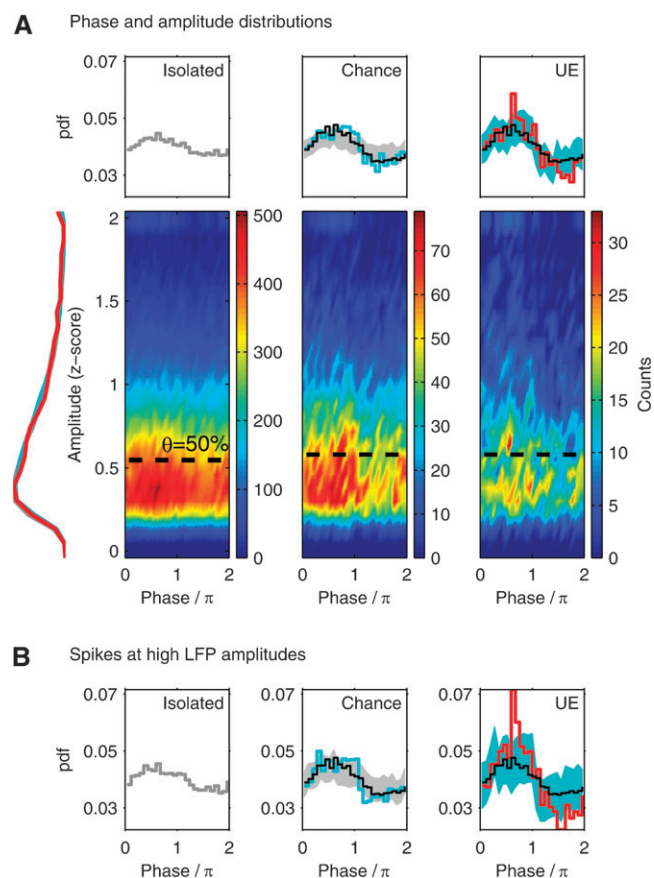

Figure 6. Relation of spike synchrony to the interplay of phase and amplitude. (A) Joint histograms of the phase and amplitude for ISO (left), CC (middle), and UE (right) pooled across the population (25 × 25 bins; color bars indicate counts; phase π indicates LFP troughs). The top and left projections display the phase and amplitude distributions, respectively. The top middle and top right graphs compare the phase distribution with the distribution shown in the graph to the left: The shaded areas enclose at each phase 95% of 1000 phase distributions randomly chosen from the set to the left with the same number of spikes as in the current set. Black curves are the predictions based on the phase distributions of the individual neurons (Ψ_{PHASE}). The histograms include the neurons which have a minimal spike count (total of 25 spikes and a mean rate of 5 Hz per trial) and for which the phase distribution of all spikes is significantly locked ($\alpha = 0.05$). (B) Phase distributions of the 3 sets, considering only the 50% of the spikes at highest LFP amplitudes (Hi spikes, $\theta = 50\%$, above dashed black lines in A).

Figure 5. Distributions of LFP phase and amplitude extracted at the spike times of a single neuron. Same neuron as in Figures 2 and 4. All distributions are normalized to unit area and are shown separately for ISO (left), CC (middle), and UE (right). (A) The modulation of the 3 phase distributions increases from left to right. Phase π is the location of the trough of the LFP oscillation. The black curve in the middle and the right graph is the predictor based on the individual phase distributions of the contributing neurons (Ψ_{PHASE}). (B) LFP amplitudes are expressed as z-score.

per trial (Supplementary Fig. S2A3,A4). Moreover, removing those spikes (12%) from the 3 sets that occur in quick succession (within 6 ms) of a previous spike in each of the 3 sets yields a similar qualitative result for the locking (Supplementary Fig. S5B). Taken together, despite the impossibility to remove the substantial fraction of coincidences originating by chance from the UE group, the locking of UE cannot be explained on the basis of the intrinsic phase locking of the neurons forming the coincidences as in the case of CC.

Magnitude of LFP Oscillation Influences Spike Locking

Earlier studies (e.g., Murthy and Fetz 1996b) demonstrate that spikes occurring during periods of high LFP amplitudes exhibit a stronger locking to the LFP. At a given time the amplitude of the LFP oscillation is defined by its envelope (blue curves in Fig. 4A). To examine the dependence of spike locking on the amplitude of the LFP (Denker et al. 2007), we form 2 exclusive sets of spikes, termed "Hi" and "Lo," based on whether a spike occurs at an amplitude above or below a certain value, respectively (Fig. 7A). We account for the session-by-session variability of the LFP amplitude by defining the threshold θ in
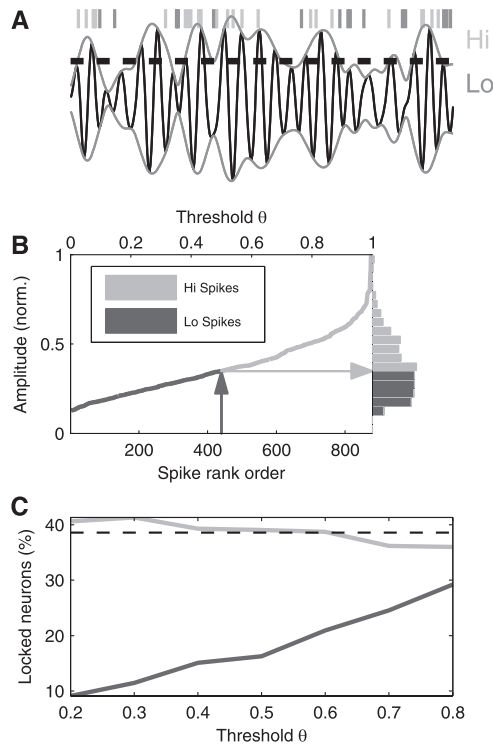

Figure 7. Influence of oscillation magnitude on locking of spikes to LFP. (A) Spikes in periods with an LFP amplitude (i.e., envelope of LFP, light gray curve) above a certain threshold (dashed line) are termed the "Hi" set (light gray ticks) and the remainder the "Lo" set (dark gray ticks). (B) Separation of spikes into Hi and Lo for the same example neuron as in Figures 2, 4, and 5. Spikes are rank ordered according to LFP amplitude; the histogram on the right shows the distribution of the respective amplitudes (normalized to maximum). The threshold θ is defined as the fraction of spikes labeled as Lo. The dark gray arrow illustrates a threshold choice of $\theta = 0.5$ and corresponds to a relative amplitude specific to each neuron (light gray arrow). Spikes at extremely low LFP amplitudes (lowest 10%) do not enter the analysis. (C) Percentage of neurons with significant (Rayleigh test, $\alpha = 0.05$) phase locking of their Hi spikes (light gray curve) and of their Lo spikes (dark gray curve) as a function of the amplitude threshold θ. Even for large θ (0.8), the set of Hi spikes shows significant locking in 36% of the neurons, although it contains only few spikes. The dashed line shows as a reference the percentage (39%) of locked neurons computed if spikes are not separated into Hi and Lo (i.e., all spikes).

terms of the fraction of spikes an individual neuron contributes to the Lo category (Fig. 7B).

For threshold ranges between 0.2 and 0.8, we observe that the percentage of significantly locked neurons (Rayleigh test, $\alpha = 0.05$) as determined by the Hi set of spikes decays only slightly from 41% to 36% (Fig. 7C). This percentage is in the same range as the percentage of locked neurons considering all spikes (dashed line; cf. also Fig. 4B). We emphasize that even for high thresholds, where only few spikes are included, the strong locking of Hi spikes explains the percentage of locked neurons found using all spikes. In contrast, when considering spikes of the Lo set, the percentage of locked neurons starts at 9% and increases approximately linearly with θ, as spikes at increasingly higher amplitudes are included in the Lo set. This result shows that the degree of LFP phase locking exhibited by a neuron is to a large extend determined by spikes that occur at high LFP amplitudes.

Combined Effects of Synchrony and LFP Amplitude

Combination of the previous results raises the question of whether coincidences, and in particular UEs, predominantly occur at high LFP amplitudes. Figure 6A (density plots) shows the number of spikes as a function of both LFP phase and amplitude for each of the 3 sets ISO, CC, and UE. Here, CC and UE occur at similar amplitudes as ISO, even though the amplitude distributions (left) reveal a small shift toward high amplitudes for CC and UE (cf., $\theta = 50\%$ lines in 2D histograms). The phase distributions (top graphs), however, clearly show a progressive increase in the degree of phase locking from ISO to CC to UE. Finally, observing that UEs exhibit similar amplitudes to CC, we can ask the reverse question of whether at high amplitudes ISO, CC, and UE still exhibit the systematic increase in locking. Figure 6B shows that for the 50% of the spikes occurring at the largest LFP amplitudes (i.e., Hi spikes, $\theta = 50\%$, above black dashed line in Fig. 6A), the effect of improved phase locking for the UE group is strongly amplified. In contrast, the ISO and CC phase distributions do not change. Despite the differences in the degree of phase locking described so far, it is instructive to observe that the average phase exhibited by individual neurons shows a strong preference for the falling phase of the LFP independent of the LFP amplitude and of whether ISO, CC, or UE spikes are considered (Supplementary Fig. S6).

To better quantify the interplay of LFP amplitude and spike synchrony in affecting the phase locking of spikes to the LFP, we calculate the increase in locking from ISO to CC separately for spikes at all amplitudes and Hi spikes by means of the root-mean-square (RMS) value between the corresponding phase-locking distributions (Fig. 8A, left). To compensate for the different number of samples in the 4 sets of spikes entering the analysis (ISO and CC, all amplitudes and Hi), we show the distribution of RMS values obtained from 1000 resamples using a common number of samples for each of the respective phase-locking distributions. The RMS distributions obtained for all amplitude spikes and Hi spikes are nearly identical. In contrast, the increase in locking from CC to UE spikes (Fig. 8A, right) is markedly stronger for Hi spikes than for all amplitude spikes. To better resolve the dependence of modulation of phase locking with amplitude, we compute the RMS difference between the CC phase distribution and the squared ISO phase distribution (ISO^2) in an amplitude-dependent manner (Fig. 8B,

left). Here, each data point represents the mean RMS distance obtained from 1000 resamples of the 2 contributing phase distributions sampled from spikes that occur in a confined range of LFP amplitude values (horizontal axis). The ISO^2 distribution is an approximation of the predictor Ψ_{PHASE} and is obtained by squaring bin by bin the ISO phase distribution and normalizing the result to unit area. The observed difference between ISO^2 and CC is not dependent on the LFP amplitude. However, the difference between the UE and the ISO^2 phase-locking distribution (Fig. 8B, right) depends strongly on the amplitude and grows rapidly for large amplitudes (same number of data points used for resampling as in the left graph). These findings show that those coincidences in UE periods that occur during strong LFP oscillations have a disproportionate influence on UE locking, whereas the amount of increase of CC locking is little affected by the amplitude.

Discussion

In this report, we explicitly reveal how the LFP relates to precise excess spike synchrony in motor cortex. Spikes, which are emitted at the same time as spikes of other neurons, exhibit a better phase locking to the dominant beta-range LFP oscillation than those which occur in isolation. However, in time periods where the number of spike coincidences is at chance level, the quality of the locking is explained by

Figure 8. Phase locking of UEs is more strongly affected by amplitude than that of CCs. (A) Left graph: RMS differences between the CC and the ISO phase-locking distributions (25 bins) calculated for 1000 random resamples with a fixed sample size to ensure identical variability (light cyan). The distribution shown in dark cyan shows the 1000 RMS values exclusively considering spikes resampled from the Hi set. Right graph: Comparison of UE and CC phase distributions (fewer spikes are used for resampling as compared with the left graph). (B) Left graph: Mean RMS between the CC and the squared ISO distributions (ISO^2, approximate predictor Ψ_{PHASE}, see Materials and Methods) as a function of LFP amplitude (z-score). Each data point is the mean RMS obtained from 1000 comparisons of resampled ISO and CC phase distributions with a fixed sample size $n = 69$. Right graph: Comparison of the UE and ISO^2 phase distributions (same n as in the left graph). All graphs consider the same selection of neuron pairs as in Figure 6.

a predictor assuming independence of the spikes constituting a coincidence. In contrast, the pronounced locking to the LFP in time periods with a significant excess of coincident spikes (UEs) cannot be explained in this way. The probability of the occurrence of coincident spikes is only weakly influenced by changes in the magnitude of the LFP signal. Nonetheless, spikes that coincide with episodes of high LFP amplitudes are on average better locked to the LFP than those at low amplitudes. A separate analysis of these 2 factors, spike synchrony and LFP magnitude, demonstrates that the enhancement in locking of UE spikes as compared with ISO spikes is dependent on the LFP amplitude, whereas the improvement for CCs is largely independent of the amplitude. What conclusions about network dynamics and possible coding mechanisms do these results imply, in particular in the light of the distinctive role of UEs?

Features of the LFP signal correlate with external stimuli (O'Leary and Hatsopoulos 2006), behavioral aspects (Scherberger et al. 2005), internal processes (Murthy and Fetz 1996a; Roux et al. 2006: Poulet and Petersen 2008), memory (Pesaran et al. 2002; Lee et al. 2005), and attentional modulation (Fries et al. 2001; Taylor et al. 2005). In particular, several authors have elucidated the functional role of LFP oscillations in motor cortex in the beta and lower gamma range. These oscillations are only loosely correlated across trials, that is, their phase is not time locked to any external (e.g., stimulus) or internal (e.g., movement onset) event. Oscillatory beta-range LFP activity in motor cortex is a unique feature of experimental protocols including a waiting period before movement execution and has been described in relation to attentional processes, movement preparation, and motor maintenance (Murthy and Fetz 1992, 1996a; Sanes and Donoghue 1993; Baker et al. 1997; Donoghue et al. 1998; O'Leary and Hatsopoulos 2006). The oscillations typically terminate at movement onset and may well represent a top-down modulatory input from higher sensory areas (e.g., Lebedev and Wise 2000). In addition, there exists a large body of knowledge about delay-related spiking activity in motor cortical areas and its functional implication in sensorimotor integration and movement preparation (for a review, see Riehle 2005). In particular, the occurrence of transient precise spike synchrony observed among individual neurons (such as detected by the UE method) is shown to relate to behavioral aspects of the task (Riehle et al. 1997; Kilavik et al. 2009) but does not depend on the mean firing rate of the participating neurons (Grammont and Riehle 2003). Reports in various brain areas demonstrate that single neurons selectively participate in oscillatory periods of the LFP by phase locking (Eckhorn and Obermueller 1993; Baker et al. 1997; Destexhe et al. 1999; Fries et al. 2001; Lee et al. 2005), where occasionally the autocorrelations of the spike trains themselves become oscillatory (Murthy and Fetz 1996b; Lebedev and Wise 2000). Yet only a few studies relate LFP oscillations to the correlation structure of the spiking activity of multiple neurons (e.g., Murthy and Fetz 1996b; Nir et al. 2007; Womelsdorf et al. 2007), most of which concentrate on interaction on the slower time scale of rates. However, the apparent complexity of the simultaneous coding of neuronal activity for different aspects of motor cortical processing challenges the idea that LFP oscillations and the emergence of transient UEs may represent 2 reflections of only one single functional process performing the planning and preparation of movements.
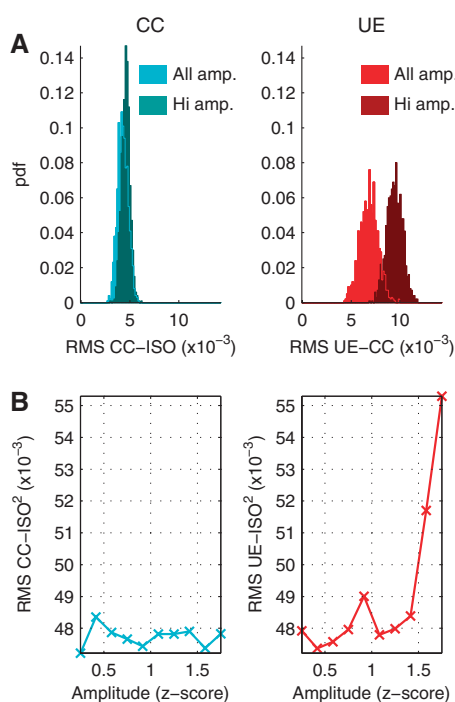
We interpret the observed excess synchrony as the result of the specific and reliable coactivation of the neurons as part of an assembly. An alternate hypothesis states that strong non-stationarities of the firing rates are the cause for false-positive detections of UE periods, which could explain the observed phase locking of UE if rates were comodulated with the LFP oscillation cycles. To investigate this possibility, we reanalyzed the data by replacing the parametric distribution implementing the null hypothesis in the original UE analysis by a distribution derived from surrogates. The employed surrogate method (spike train dithering, see Grün 2009) closely preserves the rate profiles and the interspike interval distributions and leads to a conservative (Louis et al. 2010) classification of excess synchronous events. Despite the decreased sensitivity of the surrogate-based method to detect excess synchrony, our analysis confirms the phase distributions for ISO, CC, and UE which are the essential finding of our study. Thus, they are not explained as a consequence of rate covariations but express excess synchrony as a reflection of coordinated network activity.

Our study shows that the selection of UE periods leads to an increased degree of locking of coincident spikes. A valid concern is that this selection process may influence other features of spike trains or the LFP, such that the increased locking of UE coincidences can be attributed to a more basic cause. An extensive analysis of periods classified as CC or UE does not reveal any evidence for differences in either of the 2 recorded signals: LFPs show a similar frequency and amplitude content in the 2 selections, and the rate, variability, and regularity of spike trains remains unchanged (Supplementary Fig. S2). In particular, we verified that the general degree of locking between spikes and LFP is not dependent on the separation into CC and UE sections by calculating the predictor for CCs separately from those ISO spikes that occur in CC and those in UE periods. These predictors likewise explain the locking of CC coincidences but fail to explain the locking of coincidences in UE periods (not shown).

It is therefore reasonable to assume that synchrony on a spike-by-spike level, and population oscillations expressed by the LFP both originate from network processes that involve the pulsed synchronous coactivation of specific subsets of neurons. One may argue that in this case, we should observe an even more distinct relationship between the 2 measures as seen in our data. However, our techniques to detect synchrony related to the activation of neuronal assemblies are limited. The UE analysis assesses indirectly which coincidences are more likely to originate from such activations based on the comparison of the time-resolved rate of observed and expected coincidences. Nevertheless, the set of UEs may be composed of coincidences resulting from assembly activation and a considerable fraction of CCs (see estimate below). Therefore, although the difference in locking precision between significant (UE) and nonsignificant (CC) time segments seems small at first glance, in this light it is even more surprising that we are able to detect an enhanced phase locking for the UEs. The argument implies that the subset of coincidences caused by assembly activation has a tight locking to the LFP. The conclusion that transient contributions to the LFP rather than its overall wave form are related to the generation of spike synchrony is supported by previous work demonstrating that coherent membrane potential oscillations do not generate synchronized output spikes, and that brief, simultaneous synaptic inputs to a cell are the

likely drive for action potential generation (Poulet and Petersen 2008).

The consistency of the phase at which UE spike locking is increased suggests that UEs prefer a limited range of phases of the LFP oscillation, a signal which is rather homogeneous across the motor cortex (Murthy and Fetz 1996a; Rubino et al. 2006). Although within this limited range of phases our analysis is probably not sensitive enough to resolve any differences of the preferred phase between different UE periods, the former finding renders unlikely a model of processing where assemblies can be simultaneously active and still distinguished (multiplexed) by locking to different phases of the complete oscillatory cycle (e.g., Womelsdorf et al. 2007). In such a model, we would observe shifts of the preferred phase as different assemblies become active, whereas in our data, we observe a locking increase at a specific fixed phase. Our results rather suggest that neurons participate in different assemblies at different times (see also Riehle et al. 1997) but predominantly at the same phase of the LFP (cf., Singer 1999). This view is consistent within the framework of excitatory–inhibitory loops (Berens et al. 2008), which have been suggested as a mechanism underlying oscillations (Klausberger et al. 2003; Hasenstaub et al. 2005; Cardin et al. 2009) and could temporally gate the activity within the network (Buzsáki and Draguhn 2004). Using the UE method we analyze expressions of assembly activity in 20–30% of the neurons (cf. Supplementary Fig. S4), which is in rough agreement with early estimates of the likelihood to observe significant cross-correlations (e.g., Murthy and Fetz 1996b). However, even in this subset of neurons, we can attribute only a fraction of spikes to assembly activation. One hypothesis is that the motor cortex employs parallel coding schemes, where assembly-related synchronous activity occurring at specific time points defined by the LFP phase can be dissociated from activity less localized in time, for example, realizing a rate code.

To better understand the implications for the organization of cortical processing, we consider a conceptual model where spikes of a neuronal assembly are locked to the LFP (Fig. 9) based on 1) the assumption that UEs reflect assembly activity (Riehle et al. 1997) and 2) our observation that UEs have the strongest locking to the LFP. A potential mechanism is that assembly spikes originate from synchronous synaptic input to local groups of neurons. The simplest explanation for the finding that ISO and CC also exhibit locking, albeit weaker than UE, is that the spikes of a neuron are composed of a mixture of nonassembly (unlocked) and assembly spikes (locked). The latter are not identified as UE due to the lack of corresponding partner neurons in the recording (Fig. 9A). Consequently, the phase histogram of the ISO spikes is a superposition of the histograms of nonassembly and assembly spikes, with a factor γ determining their ratio (Fig. 9B, top row). CCs are composed of spikes from independent sources (Fig. 9B, middle row) but the combinatorics of nonassembly and assembly spikes enhances the locking. Finally, periods identified as UE contain excess coincidences (Fig. 9B, bottom row) resulting from the activation of an assembly in which both neurons participate. Their relative contribution β leads to an enhanced locking of UE compared with CC. The structure of the model allows us to derive estimates of the parameters γ and β: By comparing the experimental phase distributions of CC and UE, we determine the minimal β consistent with the data. As the minimal β requires maximal locking of assembly spikes, this

simultaneously yields a minimal estimate of γ (compare Fig. 9*B*; for theoretical framework, see Denker et al. 2010). We find that outside of UE periods $\gamma = 13\%$ of the spikes of a neuron participate in an assembly and $\beta = 24\%$ of the coincidences in UE periods result from the joint participation in an assembly. Even though this is clearly a highly simplified model, it provides a quantitative bridge between functionally relevant spike synchrony (Riehle et al. 1997; Singer 1999; Maldonado et al. 2008) and the LFP as a robust mesoscopic measure of brain activity (Mehring et al. 2003).

Our results show that neuronal mass signals like the LFP convey specific information about network processes. We directly demonstrate in the brain of a behaving animal that the LFP is related to excess spike synchronization. Nevertheless, there is a substantial fraction of spikes without an apparent relationship to the LFP. Thus, the 2 measures are observables of the same neuronal network but do not necessarily carry the same information. Taken together, we interpret our results as evidence that LFP (beta) oscillations, especially at high amplitudes, are reflections of the activation of neuronal assemblies which propagate a synchronous volley through the network. Complementing recent advances in tackling the

experimental (Nicolelis et al. 1997; Euston et al. 2007; Fujisawa et al. 2008) and theoretical (Brown et al. 2004; Grün 2009) difficulties in finding signatures of coordinated activity in spike data alone, these findings indicate how the LFP may provide an additional source of information to characterize the neuronal population dynamics. With massively parallel recordings becoming available we may be able to disambiguate the superposition of multiple neuronal assemblies. This gives us confidence that by improving our understanding of the various components of the LFP signal we will eventually be able to use the LFP as an antenna delivering news from several communicating network stations.

Figure 9. Conceptual model relating increased LFP locking and assemblies. (*A*) Sketch of the LFP (top) and the simultaneous spiking activity of 5 neurons (middle), of which only 2 are recorded (yellow background). Based on the latter, time periods are distinguished where coincidences occur at chance level (non-UE, left) from those with excess synchrony (UE, right). Each spike is either part of an assembly of coactive neurons (green) or not (black). In this simplified scenario, one assembly is active during non-UE, and a different one during UE; both observed neurons contribute to the latter. Assembly spikes are assumed to exhibit locking to the LFP, expressed by a nonuniform phase distribution $p(\phi)$ (green), in contrast to the unlocked nonassembly spikes (black). (*B*) Two factors β and γ determine the composition of the phase distributions (left) for ISO, CC, and UE of assembly and nonassembly spikes. γ determines the overall probability that a spike is part of an assembly activation (top, $p_{ISO}(\phi)$). $p_{CC}(\phi)$ (middle) results from the combinatorics of spikes drawn independently from $p_{ISO}(\phi)$. $p_{UE}(\phi)$ (bottom) differs from $p_{CC}(\phi)$ by the relative excess β of assembly spikes in UE periods. An estimate of β is obtained as a function of $p^2(\phi)$ by substituting $p_{UE}(\phi)$ and $p_{CC}(\phi)$ in the bottom equation by the experimental distributions. γ is determined from either of the top 2 equations by using $p(\phi)$.

References

Aertsen AM, Gerstein GL, Habib MK, Palm G. 1989. Dynamics of neuronal firing correlation: modulation of "effective connectivity. J Neurophysiol. 61:900–917.

Baker SN, Olivier E, Lemon RN. 1997. Coherent oscillations in monkey motor cortex and hand muscle EMG show task-dependent modulation. J Physiol. 501:225–241.

Berens P, Keliris GA, Ecker AS, Logothetis NK, Tolias AS. 2008. Feature selectivity of the gamma-band of the local field potential in primate primary visual cortex. Front Neurosci. 2:199–207.

Boashash B. 1992. Estimating and interpreting the instantaneous frequency of a signal. I. Fundamentals. Proc IEEE. 80:520–538.

Brown EN, Kass RE, Mitra PP. 2004. Multiple neural spike train data analysis: state-of-the-art and future challenges. Nat Neurosci. 7:456–461.

Buzsáki G. 2004. Large-scale recording of neuronal ensembles. Nat Neurosci. 7:446.

Buzsáki G, Draguhn A. 2004. Neuronal oscillations in cortical networks. Science. 304:1926–1929.

Cardin JA, Carlén M, Meletis K, Knoblich U, Zhang F, Deisseroth K, Tsai L-H, Moore CI. 2009. Driving fast-spiking cells induces gamma rhythm and controls sensory responses. Nature. 459:663–667.

Canolty RT, Ganguly K, Kennerley SW, Cadieu CF, Koepsell K, Wallis JD, Carmena JM. 2010. Oscillatory phase coupling coordinates anatomically dispersed functional cell assemblies. Proc Natl Acad Sci U S A. 107:17356–17361.

Denker M, Riehle A, Diesmann M, Grün S. 2010. Estimating the contribution of assembly activity to cortical dynamics from spike and population measures. J Comput Neurosci. 29:599–613.

Denker M, Roux S, Timme M, Riehle A, Grün S. 2007. Phase synchronization between LFP and spiking activity in motor cortex during movement preparation. Neurocomputing. 70:2096–2101.
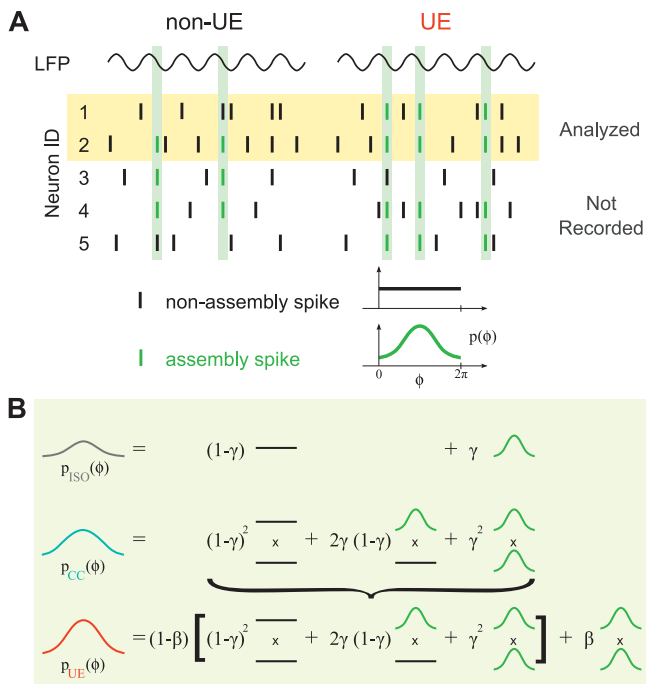
Destexhe A, Contreras D, Steriade M. 1999. Spatiotemporal analysis of local field potentials and unit discharges in cat cerebral cortex during natural wake and sleep phases. J Neurosci. 19:4595–4608.

Donoghue JP, Sanes JN, Hatsopoulos NG, Gaál G. 1998. Neural discharge and local field potential oscillations in primate motor cortex during voluntary movements. J Neurophysiol. 79:159–173.

Eckhorn R, Bauer R, Jordan W, Brosch M, Kruse W, Munk M, Reitboeck HJ. 1988. Coherent oscillations: a mechanism of feature linking in the visual cortex? Multiple electrode and correlation analyses in the cat. Biol Cybern. 60:121–130.

Eckhorn R, Obermueller A. 1993. Single neurons are differently involved in stimulus-specific oscillations in cat visual cortex. Exp Brain Res. 95:177–182.

Eeckman FH, Freeman WJ. 1990. Correlations between unit firing and EEG in the rat olfactory system. Brain Res. 528:238–244.

Elul R. 1971. The genesis of the EEG. Int Rev Neurobiol. 15:227–272.

Engel AK, König P, Gray CM, Singer W. 1990. Stimulus-dependent neuronal oscillations in cat visual cortex: inter-columnar interaction as determined by cross-correlation analysis. Eur J Neurosci. 2:588–606.

Euston DR, Tatsuno M, McNaughton BL. 2007. Fast-forward playback of recent memory sequences in prefrontal cortex during sleep. Science. 318:1147–1150.

Friedrich RW, Habermann CJ, Laurent G. 2004. Multiplexing using synchrony in the zebrafish olfactory bulb. Nat Neurosci. 7:862–871.

Fries P, Nikolić D, Singer W. 2007. The gamma cycle. Trends Neurosci. 30:309–316.

Fries P, Reynolds JH, Rorie AE, Desimone R. 2001. Modulation of oscillatory neuronal synchronization by selective visual attention. Science. 291:1560–1563.

Fujisawa S, Amarasingham A, Harrison MT, Buzsáki G. 2008. Behavior-dependent short-term assembly dynamics in the medial prefrontal cortex. Nat Neurosci. 11:823–833.

Gerstein GL, Bedenbaugh P, Aertsen MH. 1989. Neuronal assemblies. IEEE Trans Biomed Eng. 36:4–14.

Grammont F, Riehle A. 2003. Spike synchronization and firing rate in a population of motor cortical neurons in relation to movement direction and reaction time. Biol Cybern. 88:360–373.

Gray CM, König P, Engel AK, Singer W. 1989. Oscillatory responses in cat visual cortex exhibit inter-columnar synchronization which reflects global stimulus properties. Nature. 338:334–337.

Grün S. 2009. Data driven significance estimation of precise spike correlation. J Neurophysiol. 101:1126–1140.

Grün S, Diesmann M, Aertsen A. 2002a. Unitary events in multiple single-neuron spiking activity: I. detection and significance. Neural Comput. 14:43–80.

Grün S, Diesmann M, Aertsen A. 2002b. Unitary events in multiple single-neuron spiking activity: II. Nonstationary data. Neural Comput. 14:81–119.

Grün S, Diesmann M, Grammont F, Riehle A, Aertsen A. 1999. Detecting unitary events without discretization of time. J Neurosci Methods. 94:67–79.

Grün S, Riehle A, Diesmann M. 2003. Effect of cross-trial nonstationarity on joint-spike events. Biol Cybern. 88:335–351.

Hatsopoulos N, Geman S, Amarasingham A, Bienenstock E. 2003. At what time scale does the nervous system operate? Neurocomputing. 52–54:25–29.

Harris KD, Henze DA, Hirase H, Leinekugel X, Dragoi G, Czurkó A, Buzsáki G. 2002. Spike train dynamics predicts theta-related phase precession in hippocampal pyramidal cells. Nature. 417:738–741.

Hasenstaub A, Shu Y, Haider B, Kraushaar U, Duque A, McCormick DA. 2005. Inhibitory postsynaptic potentials carry synchronized frequency information in active cortical networks. Neuron. 47:423–435.

Hebb DO. 1949. The organization of behavior: a neuropsychological theory. New York: Wiley.

Ikegaya Y, Aaron G, Cossart R, Aronov D, Lampl I, Ferster D, Yuste R. 2004. Synfire chains and cortical songs: temporal modules of cortical activity. Science. 304:559–564.

Jensen O. 2006. Maintenance of multiple working memory items by temporal segmentation. Neuroscience. 139:237.

Katzner S, Nauhaus I, Benucci A, Bonin V, Ringach DL, Carandini M. 2009. Local origin of field potentials in visual cortex. Neuron. 61:35–41.

Kayser C, Montemurro MA, Logothetis NK, Panzeri S. 2009. Spike-phase coding boosts and stabilizes information carried by spatial and temporal spike patterns. Neuron. 61:597–608.

Kilavik BE, Confais J, Ponce-Alvarez A, Diesmann M, Riehle A. 2010. Evoked potentials in motor cortical local field potentials reflect task timing and behavioral performance. J Neurophysiol. 104:2338–2351.

Kilavik BE, Roux S, Ponce-Alvarez A, Confais J, Grün S, Riehle A. 2009. Long-term modifications in motor cortical dynamics induced by intensive practice. J Neurosci. 29:12653–12663.

Klausberger T, Magill PJ, Márton LF, Roberts JDB, Cobden PM, Buzsáki G, Somogyi P. 2003. Brain-state- and cell-type-specific firing of hippocampal interneurons in vivo. Nature. 421:844–848.

Lampl I, Reichova I, Ferster D. 1999. Synchronous membrane potential fluctuations in neurons of the cat visual cortex. Neuron. 22:361–374.

Lebedev MA, Wise SP. 2000. Oscillations in the premotor cortex: single-unit activity from awake, behaving monkeys. Exp Brain Res. 130:195–215.

Lee H, Simpson GV, Logothetis NK, Rainer G. 2005. Phase locking of single neuron activity to theta oscillations during working memory in monkey extrastriate visual cortex. Neuron. 45:147–156.

Le Van Quyen V, Foucher J, Lachaux J, Rodriguez E, Lutz A, Martinerie J, Varela FJ. 2001. Comparison of Hilbert transform and wavelet methods for the analysis of neuronal synchrony. J Neurosci Methods. 111:83–98.

Logothetis NK, Wandell BA. 2004. Interpreting the BOLD signal. Annu Rev Physiol. 66:735–769.

Louis S, Borgelt C, Grün S. 2010. Generation and selection of surrogate methods for correlation analysis. In: Grün S, Rotter S, editors. Analysis of parallel spike trains. New York (NY): Springer.

Maldonado P, Babul C, Singer W, Rodriguez E, Berger D, Grün S. 2008. Synchronization of neuronal responses in primary visual cortex of monkeys viewing natural images. J Neurophysiol. 100:1523–1532.

Mardia KV, Jupp PE. 2000. Directional statistics. Chichester (UK): John Wiley & Sons Ltd.

Mehring C, Rickert J, Vaadia E, de Oliveira SC, Aertsen A, Rotter S. 2003. Inference of hand movements from local field potentials in monkey motor cortex. Nat Neurosci. 6:1253–1254.

Mitzdorf U. 1985. Current source-density method and application in cat cerebral cortex: investigation of evoked potentials and EEG phenomena. Physiol Rev. 65:37–100.

Montemurro MA, Rasch MJ, Murayama Y, Logothetis NK, Panzeri S. 2008. Phase-of-firing coding of natural visual stimuli in primary visual cortex. Curr Biol. 18:375–380.

Murthy VN, Fetz EE. 1992. Coherent 25- to 35-Hz oscillations in the sensorimotor cortex of awake behaving monkeys. Proc Natl Acad Sci U S A. 89:5670–5674.

Murthy VN, Fetz EE. 1996a. Oscillatory activity in sensorimotor cortex of awake monkeys: synchronization of local field potentials and relation to behavior. J Neurophysiol. 76:3949–3967.

Murthy VN, Fetz EE. 1996b. Synchronization of neurons during local field potential oscillations in sensorimotor cortex of awake monkeys. J Neurophysiol. 76:3968–3982.

Nauhaus I, Busse L, Carandini M, Ringach DL. 2009. Stimulus contrast modulates functional connectivity in visual cortex. Nat Neurosci. 12:70–76.

Nawrot MP, Boucsein C, Rodriguez-Molina V, Riehle A, Aertsen A, Grün S, Rotter S. 2008. Measurement of variability dynamics in cortical spike trains. J Neurosci Methods. 169:374–390.

Nicolelis MA, Ghazanfar AA, Faggin BM, Votaw S, Oliveira LM. 1997. Reconstructing the engram: simultaneous, multisite, many single neuron recordings. Neuron. 18:529–537.

Nir Y, Fisch L, Mukamel R, Gelbard-Sagiv H, Arieli A, Fried I, Malach R. 2007. Coupling between neuronal firing rate, gamma LFP, and BOLD fMRI is related to interneuronal correlations. Curr Biol. 17:1275–1285.

Ohiorhenuan IE, Mechler F, Purpura KP, Schmid AM, Hu Q, Victor JD. 2010. Sparse coding and higher-order correlations in fine-scale cortical networks. Nature. 466:617-621.

Okun M, Nain A, Lampl I. 2010. The subthreshold relation between cortical local field potential and neuronal firing unveiled by intracellular recordings in awake rats. J Neurosci. 20:4440-4448.

O'Leary JG, Hatsopoulos NG. 2006. Early visuomotor representations revealed from evoked local field potentials in motor and premotor cortical areas. J Neurophysiol. 96:1492-1506.

Pesaran B, Pezaris JS, Sahani M, Mitra PP, Andersen RA. 2002. Temporal structure in neuronal activity during working memory in macaque parietal cortex. Nat Neurosci. 5:805-811.

Poulet JFA, Petersen CCH. 2008. Internal brain state regulates membrane potential synchrony in barrel cortex of behaving mice. Nature. 454:881-885.

Riehle A. 2005. Preparation for action: one of the key functions of the motor cortex. In: Riehle A, Vaadia E, editors. Motor cortex in voluntary movements: a distributed system for distributed functions. Boca Raton (FL): CRC-Press. p. 213-240.

Riehle A, Grün S, Diesmann M, Aertsen A. 1997. Spike synchronization and rate modulation differentially involved in motor cortical function. Science. 278:1950-1953.

Roux S, Mackay WA, Riehle A. 2006. The pre-movement component of motor cortical local field potentials reflects the level of expectancy. Behav Brain Res. 169:335-351.

Rubino D, Robbins KA, Hatsopoulos NG. 2006. Propagating waves mediate information transfer in the motor cortex. Nat Neurosci. 9:1549-1557.

Saleh M, Reimer J, Penn R, Ojakangas CL, Hatsopoulos NG. 2010. Fast and slow oscillations in human primary motor cortex predict oncoming behaviorally relevant cues. Neuron. 65:461-471.

Sanes JN, Donoghue JP. 1993. Oscillations in local field potentials of the primate motor cortex during voluntary movement. Proc Natl Acad Sci U S A. 90:4470-4474.

Scherberger H, Jarvis MR, Andersen RA. 2005. Cortical local field potential encodes movement intentions in the posterior parietal cortex. Neuron. 46:347-354.

Shlens J, Field GD, Gauthier JL, Grivich MI, Petrusca D, Sher A, Litke AM, Chichilnisky EJ. 2006. The structure of multi-neuron firing patterns in primate retina. J Neurosci. 26:8254-8266.

Shmiel T, Drori R, Shmiel O, Ben-Shaul Y, Nadasdy Z, Shemesh M, Teicher M, Abeles M. 2005. Neurons of the cerebral cortex exhibit precise interspike timing in correspondence to behavior. Proc Natl Acad Sci U S A. 102:18655-18657.

Singer W. 1999. Neuronal synchrony: a versatile code for the definition of relations? Neuron. 24:49-65.

Taylor K, Mandon S, Freiwald WA, Kreiter AK. 2005. Coherent oscillatory activity in monkey area v4 predicts successful allocation of attention. Cereb Cortex. 5:1424-1437.

Tetzlaff T, Rotter S, Stark E, Abeles M, Aertsen A, Diesmann M. 2008. Dependence of neuronal correlations on filter characteristics and marginal spike train statistics. Neural Comput. 20: 2133-2184.

Tiesinga P, Sejnowski TJ. 2009. Cortical enlightenment: are attentional gamma oscillations driven by ING or PING? Neuron. 63:727-732.

Vaadia E, Haalman I, Abeles M, Bergman H, Prut Y, Slovin H, Aertsen A. 1995. Dynamics of neuronal interaction in monkey cortex in relation to behavioral events. Nature. 373:515-518.

Viswanathan A, Freeman RD. 2007. Neurometabolic coupling in cerebral cortex reflects synaptic more than spiking activity. Nat Neurosci. 10:1308-1312.

Womelsdorf T, Schoffelen J, Oostenveld R, Singer W, Desimone R, Engel AK, Fries P. 2007. Modulation of neuronal interactions through neuronal synchronization. Science. 316:1609-1612.

Zanos TP, Mineault PJ, Pack CC. 2011. Removal of spurious correlations between spikes and local field potentials. J Neurophysiol. 105:474-486.